Acta Crystallographica Section A
**Foundations of Crystallography**
ISSN 0108-7673

Received 24 August 2007
Accepted 2 November 2007



# Stability of ferroic phases in the highly piezoelectric $Pb(Zr_xTi_{1-x})O_3$ ceramics

**Dhananjai Pandey,[a]* Akhilesh Kumar Singh[a] and Sunggi Baik[b]**

[a]School of Materials Science and Technology, Institute of Technology, Banaras Hindu University, Varanasi-221 005, India, and [b]Department of Materials Science and Engineering and Pohang Accelerator Laboratory, Pohang University of Science and Technology, Pohang 790-784, Republic of Korea. Correspondence e-mail: dpandey@bhu.ac.in

The morphotropic phase boundary in the phase diagram of the technologically important $Pb(Zr_xTi_{1-x})O_3$ (PZT) ceramics has been traditionally believed to separate ferroelectric tetragonal and rhombohedral phase regions. This old picture has come under close scrutiny during the last eight years following the discovery of new monoclinic phases in the *Cm* and *Cc* space groups. This article presents a brief overview of these discoveries in which the use of multiple diffraction probes (X-ray, electron, neutron diffraction) in conjunction with physical property measurements has played a crucial role. A new phase diagram of PZT showing the stability fields of these structures below room temperature is also presented.

## 1. Introduction

$PbTiO_3$ (PT) is a well known ferroelectric material with perovskite structure. The cubic paraelectric phase of PT transforms to a tetragonal ferroelectric phase below 763 K (Jaffe *et al.*, 1971). This phase transition is accompanied by a large transformation strain (tetragonality $\eta = c/a - 1 = 0.0635$) which leads to cracking of ceramic PT bodies on cooling from the sintering temperature to the room temperature through the Curie point (763 K). In order to develop sinterable PT-based ceramics, chemical substitutions at the Pb and/or Ti sites have been attempted in the past. This search has led to the discovery of the well known $Pb(Zr_xTi_{1-x})O_3$ (PZT), $Pb(Mg_{1/3}Nb_{2/3})_xTi_{1-x}O_3$ (PMN-*x*PT), $Pb(Zn_{1/3}Nb_{2/3})_xTi_{1-x}O_3$ (PZN–*x*PT) and other similar solid-solution systems with extraordinary piezoelectric properties (Jaffe *et al.*, 1971). These piezoelectric materials are of tremendous technological importance for use as sensors and actuators (Jaffe *et al.*, 1971).

The tetragonal structure of PT in the PZT, PMN–*x*PT and PZN–*x*PT solid-solution systems is stable at room temperature up to a composition ($x$) corresponding to a nearly vertical phase boundary in the temperature ($T$) – composition ($x$) phase diagram. This phase boundary is commonly known as the morphotropic phase boundary (MPB) (Jaffe *et al.*, 1971). The dielectric constant, piezoelectric coefficients and the electromechanical coupling coefficients of these ceramics are maximized for the composition closest to the MPB. To date, there is no satisfactory explanation for this extreme response although three different models based on coexistence of phases (Isupov, 1968), lattice instability near room temperature (Mishra *et al.*, 1996) and polarization rotation (Fu & Cohen, 2000; Bellaiche *et al.*, 2000; Vanderbilt & Cohen, 2001) have been proposed.

Until 1999, the MPB was believed to separate the stability phase fields of the ferroelectric tetragonal ($F_T$) and the ferroelectric rhombohedral ($F_R$) phases with the coexistence of these phases in the MPB region (Jaffe *et al.*, 1971; Mishra *et al.*, 1997). Several new monoclinic phases have recently been discovered in the MPB region of these solid-solution systems with *Cm* (Noheda *et al.*, 1999; Noheda, Gonzalo *et al.*, 2000; Noheda, Cox *et al.*, 2000), *Cc* (Hatch *et al.*, 2002; Ranjan *et al.*, 2005) and *Pm* (Singh & Pandey, 2001, 2003; Kiat *et al.*, 2002) space groups. The sixth-order Landau theory, which successfully explained the stability of the ferroelectric tetragonal, orthorhombic and rhombohedral phases of $BaTiO_3$ and other $ABO_3$ perovskites, has been extended to eighth order (Vanderbilt & Cohen, 2001), to account for the newly discovered monoclinic phases. The eighth-order Landau theory has revealed three different monoclinic phases, commonly labelled as $M_A$, $M_B$ and $M_C$ types, with space groups *Cm*, *Cm* and *Pm*, respectively (Vanderbilt & Cohen, 2001). The $M_A$- and $M_B$-type phases have the same space group (*Cm*) but in the former $P_x = P_y > P_z$ while in the latter $P_x = P_y < P_z$, where $P_x$, $P_y$ and $P_z$ are polarization components along the pseudocubic axes. First-principles calculations on PZT have not only confirmed the presence of the monoclinic phases but have also shown that they are responsible for the maximum electromechanical response (Fu & Cohen, 2000; Bellaiche *et al.*, 2000). A unique feature of the structure of the monoclinic phases is that their polarization vector can lie anywhere in a symmetry plane in contrast to that in the tetragonal and rhombohedral phases where it could lie only along the specified crystallographic directions [001] and [111],

respectively (Noheda, Gonzalo *et al.*, 2000; Noheda, Cox *et al.*, 2000; Singh & Pandey, 2003). The polarization vector of the monoclinic phase can therefore adjust itself easily to the external electric field direction and may lead to larger electromechanical response (Fu & Cohen, 2000; Bellaiche *et al.*, 2000; Noheda, Gonzalo *et al.*, 2000; Noheda, Cox *et al.*, 2000; Vanderbilt & Cohen, 2001). The presence of these monoclinic phases also minimizes the elastic energies at the various interphase boundaries (Jin *et al.*, 2003).

The purpose of this article is to present a brief overview of these discoveries in relation to PZT in which the use of multiple diffraction probes (X-ray, electron, neutron diffraction) in conjunction with physical property measurements has played a crucial role in establishing the structure and the stability fields of the two newly discovered monoclinic phases in the *Cm* and *Cc* space groups.

## 2. Structure of the room-temperature phases

### 2.1. The old picture

The structure of PZT has until recently been believed to be tetragonal ($F_T$) and rhombohedral ($F_R$) on the Ti- and Zr-rich sides of the morphotropic phase boundary (MPB) (Jaffe *et al.*, 1971) while the two phases were reported to coexist over a range of composition across the MPB. As per the description given in the book by Jaffe *et al.* (1971), the MPB lies around $x = 0.520$. The $F_T$ phase is therefore stable for $x < 0.520$ while $F_R$ is stable for $0.52 < x < 0.62$. On increasing the Zr content beyond $x = 0.62$, a new rhombohedral phase appears in which the neighbouring oxygen octahedra are rotated in an antiphase manner about the threefold axis. The space group of this rhombohedral phase is reported to be *R*3*c* and the corresponding tilt system is $a^-a^-a^-$ in Glazer's notation (Glazer, 1972). This rhombohedral phase in the *R*3*c* space group transforms to the rhombohedral phase in the *R*3*m* space group on heating above room temperature. Accordingly, the two ferroelectric rhombohedral phases in the *R*3*m* and *R*3*c* space groups are labelled $F_R^{HT}$ and $F_R^{LT}$ (Jaffe *et al.*, 1971). The $F_R^{LT}$ phase is stable up to $x \simeq 0.94$ beyond which an antiferroelectric phase in the space group *Pbam* is stabilized, which is commonly labelled as the $A_O$ phase. The cubic paraelectric phase to which $F_T$, $F_R^{HT}$, $F_R^{LT}$ and $A_O$ phases transform is labelled as the $P_C$ phase. Thus the old PZT phase diagram contains $F_T$ (*P*4*mm*), $F_R^{HT}$ (*R*3*m*), $F_R^{LT}$ (*R*3*c*), $A_O$ (*Pbam*/*Pba*2) and $P_C$ ($Pm\bar{3}m$) phases.

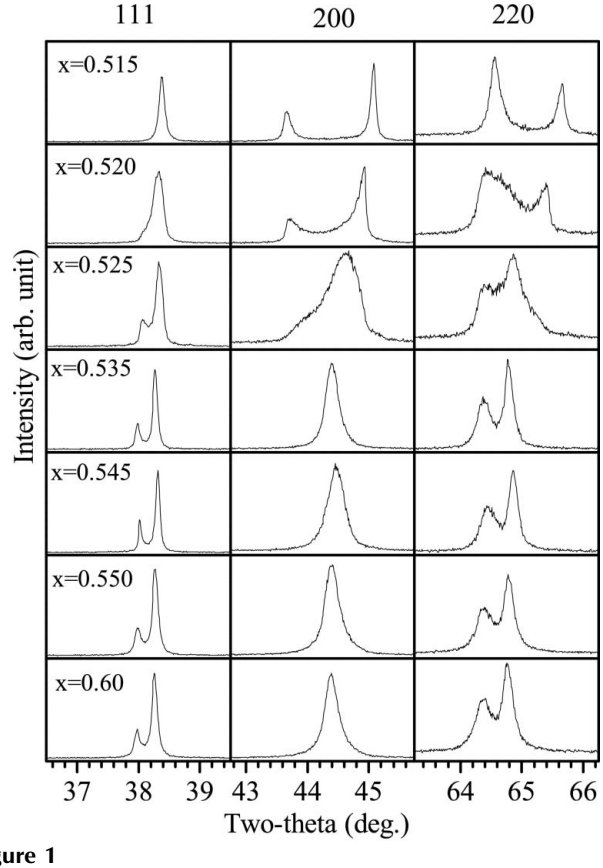


**Figure 1**
Powder synchrotron XRD profiles of 111, 200 and 220 pseudocubic reflections of PZT in the composition range 0.515 to 0.60 (after Singh *et al.*, 2007*a*).

The composition width ($\Delta x$) of the MPB depends on the preparation conditions. For example, in samples prepared by the conventional solid-state route, this width has been reported to be as small as ~0.05 (Noheda, Cox *et al.*, 2000; Schönau *et al.*, 2007) and as large as ~0.15 (Ari-Gur & Benguigui, 1974). The intrinsic width of the MPB region was shown to be much smaller, $\Delta x \simeq 0.01$, by Mishra *et al.* (1996, 1997) in chemically homogeneous samples prepared by a semi-wet route (Singh *et al.*, 1993). Fig. 1 depicts the synchrotron powder XRD profiles of the pseudocubic 111, 200 and 220 reflections of PZT prepared by the semi-wet route for different Zr content across the MPB. For the tetragonal ($F_T$) structure, the 111 profiles should be a singlet whereas the 200 and 220 are doublets. For the rhombohedral ($F_R^{HT}$) structure, the 200 is a singlet while 220 and 111 are doublets. The doublet character of 200 and 220 and singlet nature of 111 confirms the tetragonal structure for $x = 0.515$ in Fig. 1. On the other hand, the structure is apparently rhombohedral for $x > 0.525$, as 200 is now a singlet while 111 is a doublet. For $x = 0.520$ and 0.525, the diffraction profiles do not correspond to either $F_T$ or $F_R^{HT}$ phases, and this was interpreted as being due to a coexistence of the two phases (Mishra *et al.*, 1996, 1997).

### 2.2. The current picture

**2.2.1. Structure of PZT with $x = 0.525$.** The composition $x = 0.525$ was earlier regarded as consisting of coexisting T and R phases (Singh *et al.*, 1993) on the basis of the doublet nature of the 200 and 222 profiles. Recently, Ragini *et al.* (2001) carried out a Rietveld refinement for this composition using rotating-anode powder XRD data and concluded that this composition consists of a coexistence of the $F_T$ and a monoclinic phase in the *Cm* space group, earlier discovered by Noheda *et al.* (1999) below room temperature for $x = 0.520$. Full-pattern Rietveld refinements of $x = 0.525$ carried out using synchrotron powder XRD data considering coexistence of $F_R^{HT}$ and $F_T$ phases and pure monoclinic phase reveal that the structure of PZT for this

composition is nearly pure monoclinic in the *Cm* space group (Singh *et al.*, 2007*a*). The results of Rietveld refinements are illustrated using a few selected profiles in Fig. 2, from which it is evident that the pure monoclinic phase in the *Cm* space group accounts very well for the observed profiles for this composition. The refinement for the model based on the coexistence of $F_T$ and $F_R^{HT}$ phases leads to very poor fit. Consideration of the coexisting $F_T$ phase with the monoclinic phase does not lead to any statistically significant improvement in the fits (Singh *et al.*, 2007*a*). The consideration of coexisting $F_R^{HT}$ and monoclinic phases, as proposed by Frantti *et al.* (2002), on the other hand, deteriorates the fits and leads to higher $\chi^2$ (2.22) as compared to that for pure *Cm* ($\chi^2 = 2.08$) even though the number of refinable structural parameters has increased from 15 for pure *Cm* to 24 for the *Cm* + *R*3*m* model (Singh *et al.*, 2007*a*). All these facts establish the structure of PZT for $x = 0.525$ as pure monoclinic in the *Cm* space group. We label this ferroelectric monoclinic phase as the $F_M^{HT}$ phase, in analogy with the labelling of the ferroelectric rhombohedral phase in *R*3*m* space group as $F_R^{HT}$ by Jaffe *et al.* (1971). The monoclinic cell parameters ($a_m$, $b_m$, $c_m$) of $F_M^{HT}$ are related to the elementary perovskite cell parameters ($a_p$, $b_p$, $c_p$) as: $a_m \simeq \sqrt{2}\, a_p$, $b_m \simeq \sqrt{2}\, b_p$ and $c_m \simeq c_p$. The equivalent perovskite cell parameters of the $F_M^{HT}$ phase for $x = 0.525$ are $a_p \simeq 4.0681$, $b_p \simeq 4.0552$, $c_p \simeq 4.0975$, which implies that this phase is of $M_A$ type ($P_X = P_Y < P_Z$) in the notation of Vanderbilt & Cohen (2001).

**2.2.2. Structure of PZT with $x \leq 0.520$**. Rietveld refinements for $x \leq 0.515$ have confirmed the tetragonal structure in the *P*4*mm* space group but the location of the Pb atoms has been found to be disordered along the pseudocubic ⟨110⟩ directions perpendicular to the tetragonal *c* ([001]) axis (Noheda, Gonzalo *et al.*, 2000; Ragini *et al.*, 2002). These directions correspond to the [100] and [010] directions of the monoclinic $F_M^{HT}$ phase suggesting that, within the framework of the average tetragonal structure of PZT for $x < 0.520$, the local structure at the unit-cell level is indeed monoclinic like. The results of the Rietveld refinements for the intermediate composition $0.515 < x < 0.525$, *i.e.* $x = 0.520$, show that tetragonal and monoclinic phases coexist for this composition (Singh *et al.*, 2007*b*), which gives a composition width of $\Delta x \simeq 0.01$ for the phase coexistence region.

**2.2.3. Structure of PZT with $0.525 < x < 0.62$**. On increasing the Zr content beyond $x = 0.525$, the splitting of the 200 peak in Fig. 1 disappears but there is an anomalous broadening of this peak, as previously noted by Ragini *et al.* (2002) even in the rotating-anode powder XRD data. Fig. 3 shows the composition dependence of the ratio of the full widths at half-maximum (FWHM) of 200 and 111 reflections (using rhombohedral indices) obtained from the synchrotron powder XRD data. This ratio is nearly equal to 1 for the tetragonal compositions, as expected. For the rhombohedral compositions also this ratio should have been nearly equal to one but it is much larger for $x \geq 0.535$. This anomalous broadening has in the past been accounted for in the Rietveld refinements (Noheda, Gonzalo *et al.*, 2000) using anisotropic peak broadening functions proposed by Stephens (1999). However, we have recently shown that the use of the anisotropic peak broadening functions to account for the anomalous broadening of the *h*00- and *hh*0-type reflections leads to mismatch in the observed and calculated synchrotron XRD profiles for other reflections, like 111 (Singh *et al.*, 2007*a*). This is illustrated in Fig. 4(*a*). If one constrains the refinement to account for the observed width of 111 profiles, large mismatch appears for the 200 and 220 reflections (see Fig. 4*b*). For PZT compositions much richer in Zr content, Corker *et al.* (1998) have proposed that acceptable agreement factors in the Rietveld refinements using the rhombohedral space group could be obtained only if one considers off-centred displacements of the Pb atoms along the ⟨110⟩ pseudocubic directions. However, consideration of such a local disorder model in the Rietveld refinements for $x = 0.535$ did not improve the fits (see Fig. 4*c*). All these comprehensively rule out the *R*3*m* space group, with or without local disorder of Pb, for $x = 0.535$. Use

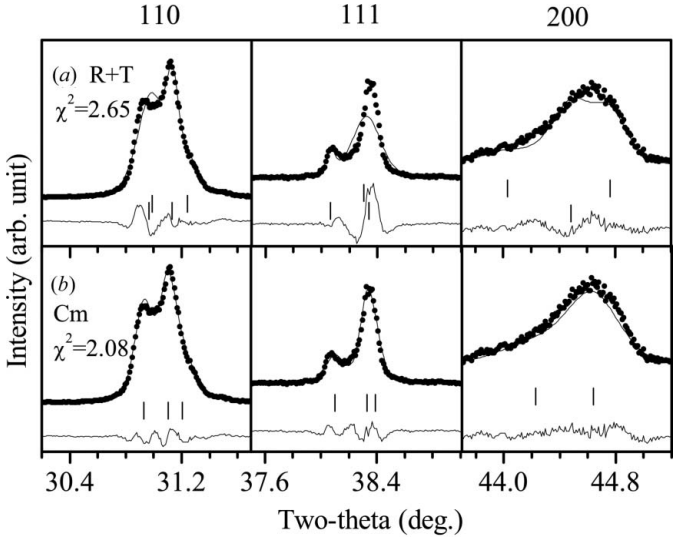


**Figure 2**
Observed (dots), calculated (continuous line) and difference (bottom line) profiles of 110, 111 and 200 pseudocubic reflections of $Pb(Zr_{0.525}Ti_{0.475})O_3$ using (*a*) coexistence of rhombohedral and tetragonal and (*b*) pure monoclinic (*Cm*) structural models. The vertical tick marks above the difference profiles give the positions of the Bragg reflections (after Singh *et al.*, 2007*a*).

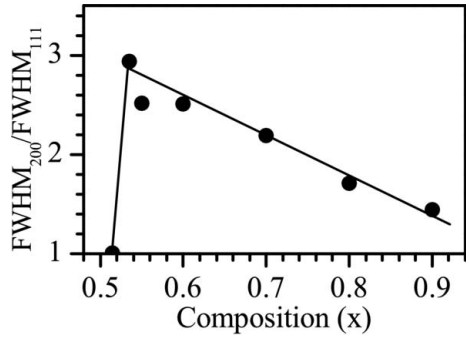


**Figure 3**
Variation of the ratio of the FWHM of the profiles of the 200 and 111 pseudocubic reflections for Zr-rich compositions of PZT (after Singh *et al.*, 2007*a*).

of the *Cm* space group, on the other hand, leads to much lower $\chi^2$ and excellent fits for both the 200- and 111-type reflections (see Fig. 4*d*). The results shown in Fig. 4 thus clearly favour the *Cm* space group for $x = 0.535$ in agreement with the earlier results of Rietveld refinements using rotating-anode XRD data (Ragini *et al.*, 2002). Similar refinements using synchrotron XRD data for higher Zr compositions revealed the inadequacy of the rhombohedral structure and the correctness of the *Cm* space group. It is thus clear that the structure of PZT at 300 K is pure monoclinic ($F_M^{HT}$) in the *Cm* space group for the composition range $0.525 \leq x \leq 0.62$ (Singh *et al.*, 2007*a*) and not rhombohedral, as hitherto believed for decades [see *e.g.* books by Jaffe *et al.* (1971), Jona & Shirane (1962) and Lines & Glass (1977)].

The variation of the equivalent elementary perovskite cell parameters with composition at 300 K for the monoclinic compositions ($x \geq 0.520$) is depicted in Fig. 5. The $a_p$ and $b_p$ lattice parameters of the monoclinic $F_M^{HT}$ phase are found to increase with composition for $0.520 \leq x < 0.545$ and then show saturation for $x \geq 0.545$. The monoclinic angle $\beta$ also increases with increasing $x$ up to $x < 0.545$ but starts decreasing for $x \geq 0.545$. The value of $c_m$ is highest for $x = 0.520$ and it decreases rather fast with $x$ before showing saturation for $x \geq 0.535$. The $c/a$ ratio decreases sharply with increasing Zr content and becomes very close to one for $x \geq 0.545$ as can be seen from the inset in Fig. 5. The unit-cell volume increases sharply for $x < 0.545$ and then increases slowly for higher Zr content (see the inset).

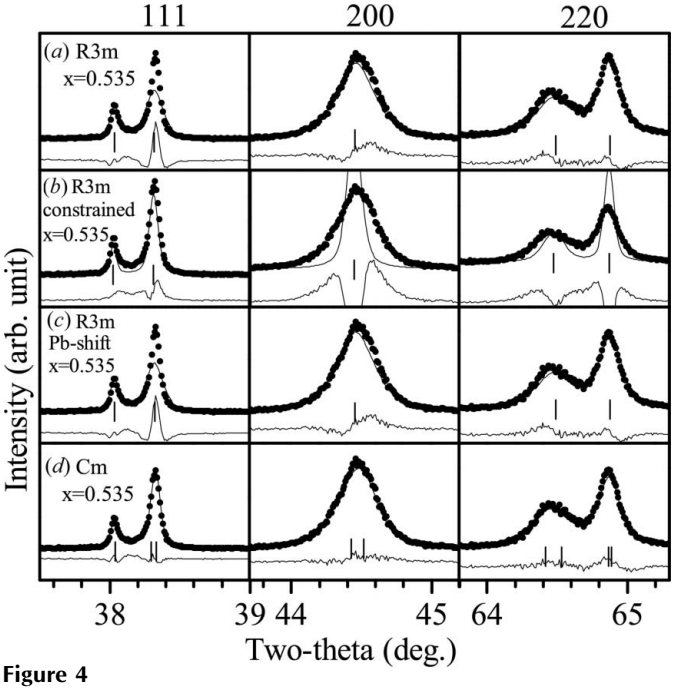


**Figure 4**
Observed (dots), calculated (continuous line) and difference (bottom line) profiles of 111, 200 and 220 pseudocubic reflections of PZT for $x = 0.535$ using various structural models. The vertical tick marks above the difference profiles give the positions of the Bragg reflections (after Singh *et al.*, 2007*a*).

**2.2.4. Structure of PZT with $0.62 < x < 0.90$.** The structure of PZT is known to change for $x > 0.62$ due to a tilt transition, driven by *R* point ($q = \frac{111}{222}$) anomaly, occurring above room temperature. Traditionally, the rhombohedral *R*3*c* space group (Jona & Shirane, 1962) in the $a^-a^-a^-$ tilt system (Clarke & Glazer, 1976; Glazer *et al.*, 1978; Corker *et al.*, 1998) has been assigned to such compositions. On heating above the room temperature, this phase (labelled $F_R^{HT}$ by Jaffe *et al.*, 1971) transforms to $F_R^{HT}$ (space group *R*3*m*). However, Corker *et al.* (1998), while refining the structure using powder neutron diffraction data, found that, unless one considers local disordered displacements of Pb in the ⟨110⟩ pseudocubic directions, the *R*3*c* space group cannot give satisfactory agreement factors. For $x = 0.90$ and 0.95, monoclinic phases in the *Pc* and *Pm* space groups have been postulated on the basis of electron diffraction patterns (Woodward *et al.*, 2005). For these compositions, superlattice reflections due to anti-phase octahedral tilting associated with *R* ($q = \frac{111}{222}$) point instability are observed in the powder neutron diffraction data (Glazer *et al.*, 1978; Corker *et al.*, 1998). Our synchrotron XRD data for compositions with $0.62 < x \leq 0.90$ reveal anomalous broadening of the 200 peak, similar to that observed in the composition range $0.530 \leq x < 0.62$, as can be seen from Fig. 3 for $x = 0.70$, 0.80 and 0.90. This anomalous broadening of the *h*00 and *hh*0 reflections and the presence of superlattice reflections can be accounted for in the *Cc* space group (tilt system $a^-a^-c^-$), which has been discovered recently at low temperatures for $x = 0.520$ (see Ragini *et al.*, 2001; Hatch *et al.*, 2002; Ranjan *et al.*, 2005; see §3.6 for more details). Fig. 6 depicts the observed and calculated profiles of the 111, 200 and 220 pseudocubic reflections, obtained after full-pattern Rietveld refinements using synchrotron XRD data in the $2\theta$

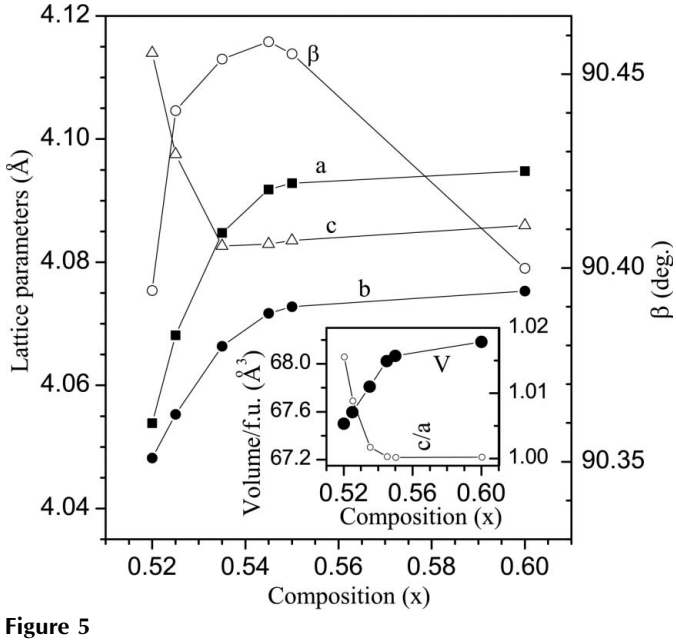


**Figure 5**
Variation of the equivalent elementary perovskite cell parameters with composition ($x$). The inset shows the cell volume and $c/a$ ratio against composition (after Singh *et al.*, 2007*a*).

range 18 to 130°. In these refinements, we have used anisotropic thermal parameters and anisotropic peak broadening functions, which account for the anomalous broadening of the 200 and 220 reflections, as can be seen from Fig. 6. However, the mismatch for the 111 peak is quite noticeable for the *R*3*c* space group, similar to that shown in Fig. 4(*a*) for *R*3*m*. Consideration of the *Cc* space group, on the other hand, accounts for all the reflections very satisfactorily. Thus, we conclude that the structure of PZT for $0.62 < x \leq 0.90$ is also monoclinic but in the *Cc* space group, which we label as $F_M^{LT}$ phase in analogy with the $F_R^{LT}$ phase given by Jaffe *et al.* (1971) for this composition range. It is worth mentioning that the neutron data used by Corker *et al.* (1998) did not have sufficient resolution to capture the anomalous broadening shown in Fig. 3. Our refinements for the *Cc* space group, which gives a better fit than the *R*3*c* space group between the observed and calculated profiles, suggest that the monoclinic order is not local at the unit-cell level as envisaged by Corker *et al.* (1998) but longer ranged, enabling the choice of a monoclinic space group in the Rietveld refinements.

## 3. The low-temperature phase transitions

### 3.1. Background

Using the piezoelectric resonance frequency ($f_r$), planar electromechanical coupling coefficient ($k_P$), and X-ray diffraction measurements, Mishra *et al.* (1997) established the following sequence of phase transitions near MPB: $F_T$ to $P_C$ for $x \leq 0.520$, $F_T + F_R \rightarrow F_T \rightarrow P_C$ for $x = 0.525$, $F_R \rightarrow F_T + F_R \rightarrow F_T \rightarrow P_C$ for $0.530 \leq x \leq 0.545$, and $F_R \rightarrow P_C$ for $x \geq 0.550$ on successively increasing the temperatures above 300 K. These studies clearly suggested that the phase coexistence at room temperature in the MPB region is due to a first-order phase transition between the low-temperature rhombohedral (stable below room temperature) and higher-temperature tetragonal phases, since even the pure $F_R$ phase for $0.530 \leq x \leq 0.545$ passed through a two-phase region consisting of $F_R$ and $F_T$ phases before transforming fully into the $F_T$ phase. Mishra *et al.* (1996) accordingly proposed that the enhanced electromechanical response near the MPB compositions is linked with the lattice instability in the vicinity of the $F_R$ to $F_T$ phase transition. Evidence for such an instability was found by Thapa (1998) in our laboratory who observed a dielectric anomaly for PZT with $x = 0.520$ below the room temperature.

### 3.2. XRD evidence for a tetragonal to monoclinic phase transition

The first structural evidence for a low-temperature phase transition was reported by Noheda *et al.* (1999) who discovered a tetragonal to monoclinic phase transition below room temperature in PZT compositions ($x = 0.520$) close to the MPB. They also confirmed that the space group of this monoclinic phase is *Cm* (Noheda, Gonzalo *et al.*, 2000). This phase transition is evidenced by the appearance of new peaks as illustrated in Fig. 7, which depicts synchrotron powder XRD profiles of the pseudocubic 200, 220 and 222 reflections of PZT with $x = 0.520$ in the temperature range 10 to 400 K. It is

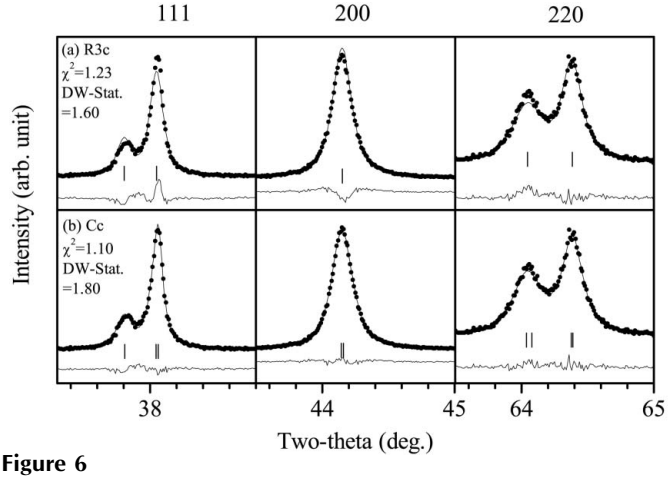


**Figure 6**
Observed (dots), calculated (continuous line) and difference (bottom line) profiles of 111, 200 and 220 pseudocubic reflections of PZT for $x = 0.70$ using (*a*) *R*3*c* and (*b*) *Cc* space groups (after Singh *et al.*, 2007*b*).

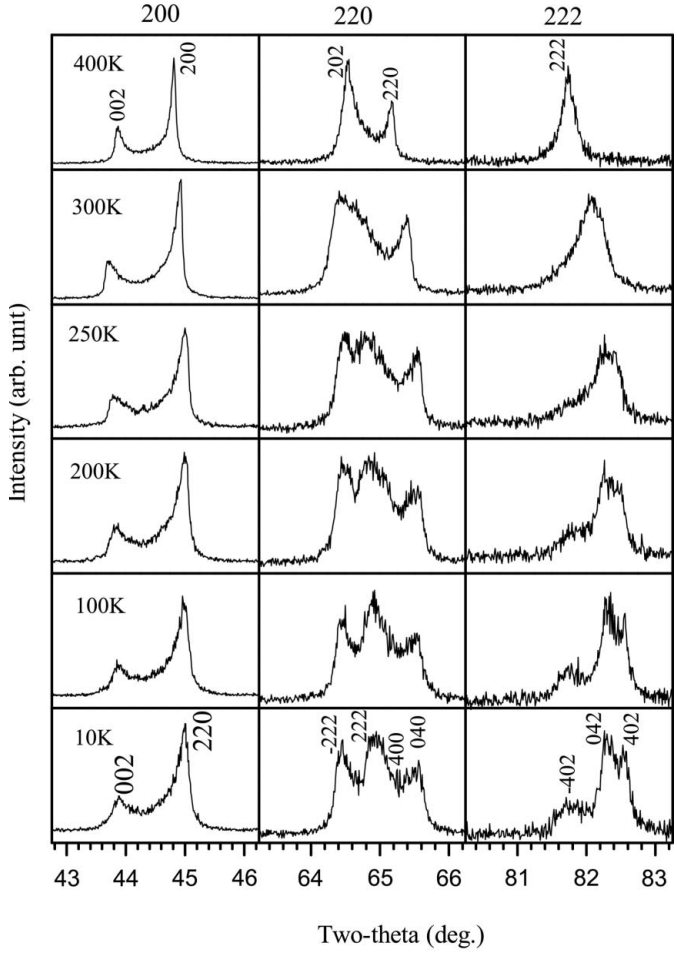


**Figure 7**
Temperature evolution of the powder synchrotron XRD profiles of 200, 220 and 222 pseudocubic reflections of PZT with $x = 0.520$. The Miller indices of the reflections shown at 10 K correspond to the monoclinic structure in the *Cm* space group.

evident from this figure that the structure is nearly tetragonal at 400 K. On cooling to 300 K, the 220 and 222 reflections show anomalous asymmetric broadening. On further cooling below room temperature, new peaks emerge. For example, the singlet 222 profile of the tetragonal phase becomes a triplet of 402, 042 and $\bar{4}02$ reflections of the monoclinic phase in the *Cm* space group. As pointed out by Noheda, Gonzalo *et al.* (2000), this monoclinic phase can be pictured as providing a 'bridge' between the $F_R$ and $F_T$ structures in the region of the MPB since the polarization vector of the monoclinic phase lies in the pseudocubic $(1\bar{1}0)$ plane, whereas the polarization vectors of the $F_R^{HT}$ and $F_T$ phases are along the [111] and [001] pseudocubic directions. This is illustrated in Fig. 8. The polar axis of the monoclinic phase for $x = 0.520$ is tilted about 24° from the [001] direction towards the [111] direction. It is interesting to note that evidence for a tetragonal-to-monoclinic phase transition in the ferroelectric $PbFe_{0.5}Nb_{0.5}O_3$ was reported by Bonny *et al.* (1997) and Lampis *et al.* (1999) using single-crystal and powder diffraction data, respectively, prior to the work of Noheda *et al.* (1999).

### 3.3. Evidence for two phase transitions in elastic modulus and dielectric studies

Soon after the report by Noheda *et al.* (Noheda *et al.*, 1999; Noheda, Gonzalo *et al.*, 2000; Noheda, Cox *et al.*, 2000) about the low-temperature tetragonal-to-monoclinic phase transition in PZT, Ragini *et al.* (2001) found evidence for one more low-temperature phase transition in poled PZT ceramics with $x = 0.515$ and 0.520 on the basis of the temperature dependence of the piezoelectric resonance frequency ($f_r$) and dielectric constant ($\varepsilon'$). The piezoelectric resonance frequency is related to the elastic modulus $(1/S_{11})$ (see Jaffe *et al.*, 1971, p. 293). The elastic modulus of normal solids which expand on heating is known to increase with decreasing temperature. However, it is evident from Fig. 9, which depicts the temperature variation of $1/S_{11}$ (as obtained from $f_r$ values) and $\varepsilon'$ for $x = 0.520$, that $1/S_{11}$ decreases with decreasing temperature up to about 260 K. Such an anomalous temperature dependence of the elastic modulus is a signature of a lattice instability due to softening of some phonon modes due to an impending structural phase transition. The temperature dependence of $1/S_{11}$ becomes normal in the temperature range 230 to 260 K, as evidenced by its increasing behaviour with decreasing temperature, revealing a phase transition around 260 K. This temperature is close to the tetragonal-to-monoclinic phase transition temperature of 250 K reported by Noheda *et al.* (1999) for $x = 0.520$ using XRD data. Intriguingly, the $1/S_{11}$ starts decreasing again anomalously on further cooling below ~230 K up to 210 K. Below 210 K, the temperature variation of $1/S_{11}$ becomes once again normal. This reveals yet another phase transition below 210 K in PZT with $x = 0.520$ for which there is no evidence in the synchrotron XRD data of Noheda *et al.* (Noheda *et al.*, 1999; Noheda, Gonzalo *et al.*, 2000; Noheda, Cox *et al.*, 2000) or the synchrotron XRD profiles on our sample shown in Fig. 7. Corresponding to these two phase transitions around 260 and 210 K, one also observes anomalies in the real part of the dielectric constant ($\varepsilon'$), as shown in Fig. 9.

### 3.4. Evidence for a superlattice phase by electron and neutron diffraction

The observation of only one phase transition in the powder XRD study of PZT with $x = 0.520$ by Noheda *et al.* (Noheda *et al.*, 1999; Noheda, Gonzalo *et al.*, 2000; Noheda, Cox *et al.*, 2000) and Ragini *et al.* (2001) and two phase transitions in the elastic modulus and dielectric studies was quite enigmatic. The first structural evidence for the lower-temperature phase transition in tetragonal PZT compositions came through electron diffraction studies by Ragini *et al.* (2001) on a PZT composition with $x = 0.515$, for which the two low-temperature phase transitions, as revealed by the elastic modulus and dielectric measurements, occur around 200 and 260 K. Fig. 10 depicts the [001] and $[10\bar{1}]$ zone selected-area electron diffraction (SAD) patterns for $x = 0.515$. It is evident from this

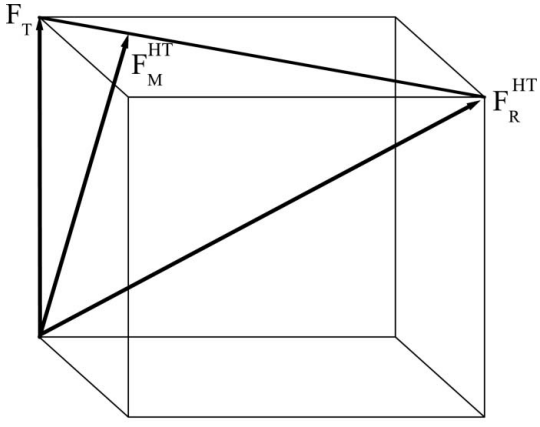


**Figure 8**
Direction of polarization vector in the $F_R^{HT}$ [111], $F_M^{HT}$ [in the plane $(\bar{1}10)$] and $F_T$ [001] phases of PZT.

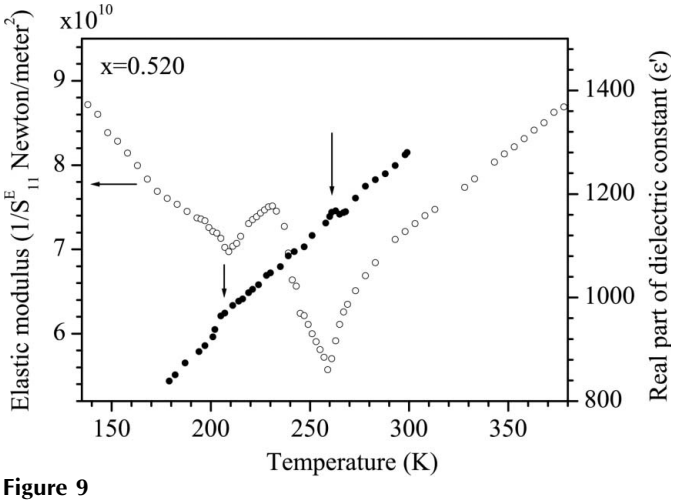


**Figure 9**
Temperature variation of the elastic modulus $(1/S_{11})$ (open circles) and real part of the dielectric constant $(\varepsilon_r')$ (filled circles) for a poled $Pb(Zr_{0.52}Ti_{0.48})O_3$ ceramic (after Ragini *et al.*, 2001).

figure that weak superlattice reflections with pseudocubic indices of the type $\frac{1}{2}$ [*hkl*] with $h, k, l = 2n + 1$ ($n$ any integer) are present in the SAD patterns recorded at 189 and 98 K. The appearance of these superlattice reflections below 219 K clearly suggests that the pseudocubic unit cell is doubled between 219 and 189 K. Since the second low-temperature anomaly in the elastic modulus and dielectric constant in PZT with $x = 0.515$ occurs at 201 K (see Ragini *et al.*, 2001), these anomalies, in the light of the electron diffraction results, are associated with a cell-doubling transition. It was shown by Ragini *et al.* (2001) that the $c$ parameter of the superlattice phase is twice the $c$ parameter of the monoclinic phase discovered by Noheda *et al.* (Noheda *et al.*, 1999; Noheda, Gonzalo *et al.*, 2000; Noheda, Cox *et al.*, 2000). Since the first report by Ragini *et al.* (2001), this superlattice phase has been subsequently confirmed in the TEM studies by Noheda *et al.* (2002) and Woodward *et al.* (2005).

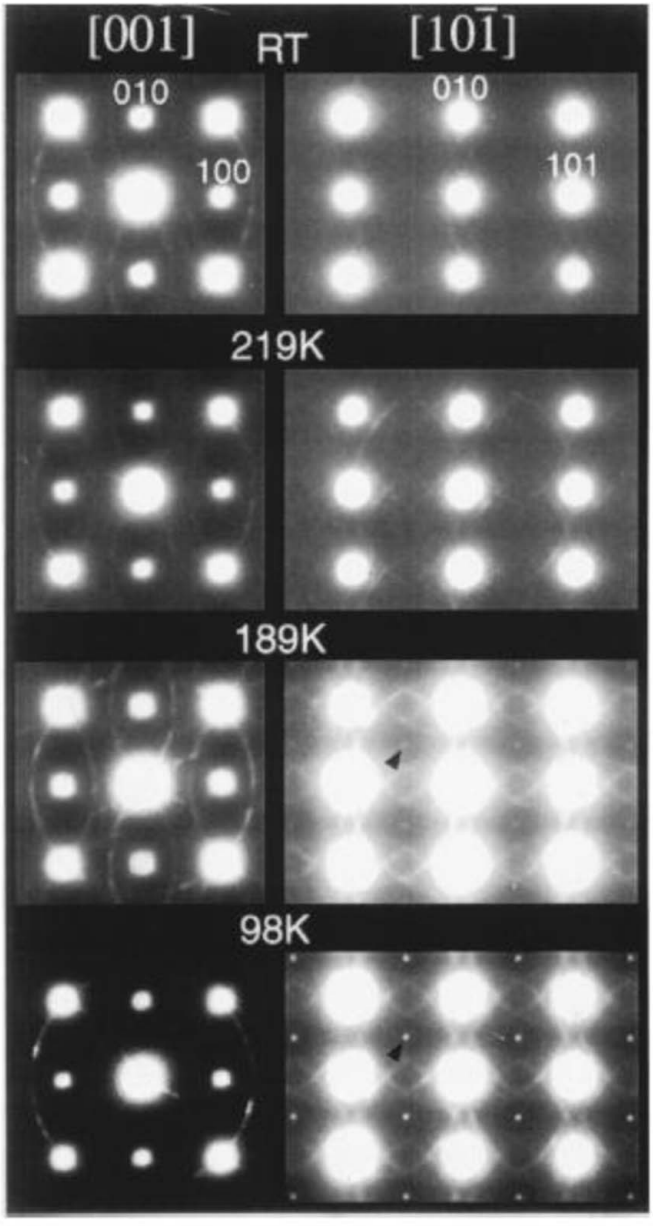


**Figure 10**
The evolution of [001] and [10$\bar{1}$] zone-axis selected-area electron diffraction patterns with temperature for PZT with $x = 0.515$. Superlattice reflections due to a cell doubling transition are seen in the 189 and 98 K patterns (after Ragini *et al.*, 2001).

Ranjan *et al.* (2002) carried out a powder neutron diffraction study of PZT with $x = 0.520$ in the temperature range 300 to 10 K. This study also confirmed the appearance of superlattice reflections which are marked with arrows in Fig. 11. These superlattice peaks cannot be indexed with respect to the *Cm* monoclinic cell. They appear at $T \leq 210$ K as can be seen from the inset to Fig. 11 which depicts the temperature evolution of one of these reflections. This temperature (~210 K) coincides with the second phase-transition temperature of PZT with $x = 0.520$ shown in Fig. 9. Indexing of all the reflections in Fig. 11, including the weak ones, requires a monoclinic cell whose $c$ parameter is twice that of the monoclinic phase reported by Noheda *et al.* (Noheda *et al.*, 1999; Noheda, Gonzalo *et al.*, 2000; Noheda, Cox *et al.*, 2000). Subsequent to the work of Ranjan *et al.* (2002), superlattice reflections in the low-temperature powder neutron diffraction patterns of tetragonal PZT compositions close to MPB were reported by Frantti *et al.* (2002) and Cox *et al.* (2005) also.

### 3.5. Role of antiferrodistortive phase transition

In oxide perovskites like $SrTiO_3$ (Bruce & Cowley, 1980), $LaAlO_3$ (Howard *et al.*, 2000) and $CaTiO_3$ (Kennedy *et al.*, 1999), antiferrodistortive (AFD) structural phase transitions, involving 'anti-phase' and 'in-phase' octahedral tilts (rotations) due to the softening and freezing of the R ($q = \frac{1}{2}\frac{1}{2}\frac{1}{2}$) and M ($q = \frac{1}{2}\frac{1}{2}0$) point modes of the cubic phase, are known to lead to unit-cell doubling and appearance of superlattice reflections. These superlattice structures can be described in terms of a doubled pseudocubic cell of the type $2a_p \times 2b_p \times 2c_p$, where $a_p$, $b_p$ and $c_p$ are the unit-cell parameters of the elementary perovskite cell. With respect to such a doubled pseudocubic cell, the Miller indices of the main perovskite reflections correspond to three even (e) numbers (*i.e.*, the Miller indices are of eee type) while the superlattice

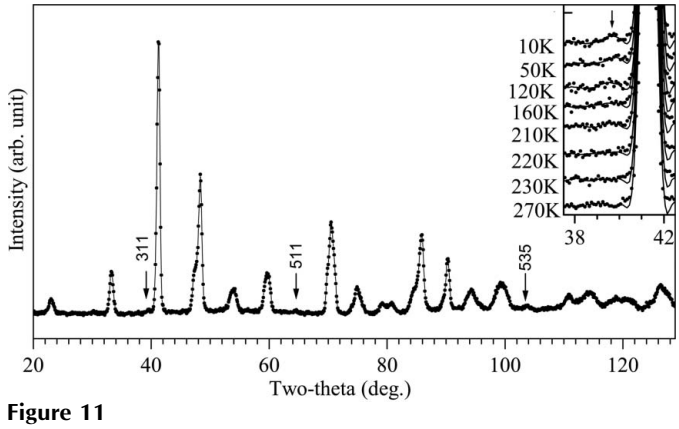


**Figure 11**
Powder neutron diffraction pattern of PZT with $x = 0.520$ at 10 K. The inset shows the evolution of the 311 superlattice reflection in the temperature range 270 to 10 K (after Ranjan *et al.*, 2002).

reflections are represented by all-odd (ooo) or two-odd and one-even (ooe) type indices depending on whether they have resulted from anti-phase (or negative) or in-phase (or positive) tilts of the neighbouring O-atom octahedra, respectively (Glazer, 1972). The Miller indices of the superlattice reflections in Fig. 11 are 311, 511 and 535, all of which are of ooo type indicating that these reflections have arisen from anti-phase (−) tilting of the neighbouring $TiO_6$ octahedra. This analysis suggests that the cell doubling transition discovered by Ragini *et al.* (2001) and Ranjan *et al.* (2002) in their electron and neutron diffraction studies is an AFD phase transition involving an *R*-point instability. This conclusion is also supported by the results of first principles density functional calculations (Fornari & Singh, 2001) which reveals a substantial *R*-point AFD instability coexisting with Γ-point ferroelectric instability for MPB compositions.

### 3.6. Structure of the superlattice phase

Ranjan *et al.* (2002) have proposed a simple model shown in Fig. 12 for the structure of the low-temperature superlattice phase. In a stack of two monoclinic cells of the *Cm* type shown in this figure, an *R*-point instability leading to $a^oa^oc^-$-type tilt will rotate the four O atoms labelled 3, 4, 5 and 6 in the $z = \frac{1}{4}$ plane and another set of four O atoms, labelled 3′, 4′, 5′ and 6′, in the $z = \frac{3}{4}$ plane in the anticlockwise and clockwise manners about the [001] direction by equal magnitude. As a result of such an anti-phase tilt about the [001] direction, the mirror planes at $y = 0, \frac{1}{2}$ of the *Cm* space group are destroyed while new *a*-glide planes appear at $y = \frac{1}{4}, \frac{3}{4}$. Further, the doubled monoclinic cell shown in Fig. 12 is a body-centred monoclinic cell. Amongst the monoclinic space groups listed in *International Tables for Crystallography*, it was found that the space group corresponding to the structural model shown in Fig. 12 is *I*1*a*1. With a new choice of axes, the space group *I*1*a*1 can equivalently be written as *Cc* in the standard setting [see *International Tables for Crystallography* (2005), Vol. A, space group No. 9]. The unit-cell axes *A*, *B*, *C* of the *Cc* space group are related to those ($a_m$, $b_m$, $c_m$) of the *Cm* space group as $A = \mathbf{a}_m + 2\mathbf{c}_m$, $B = \mathbf{b}_m$, $C = -\mathbf{a}_m$. This space group can result from the $Pm\bar{3}m$ space group by coupling the $\Gamma_4^-$ and $R_4^+$ IR's, leading to the $a^-a^-c^-$ tilt system in the *Cc* space group (Stokes & Hatch, 2000). It is interesting to note that a single anti-phase tilt $a^oa^oc^-$ about the *c* direction of the *Cm* phase considered in Fig. 12 is sufficient to reduce the symmetry to *Cc*, but the *Cc* symmetry also allows tilts in the *ab* plane to appear.

Ranjan *et al.* (2002) initially proposed a *Pc* space group for this superlattice phase which was subsequently corrected to *I*1*a*1 ≡ *Cc*, and confirmed by Rietveld refinement (Hatch *et al.*, 2002). The *Cc* space group has since been confirmed by several workers in TEM studies (Noheda *et al.*, 2002; Woodward *et al.*, 2005). Further, a recent first-principles calculation has also confirmed that the *Cc* phase is the ground state of PZT with $x = 0.520$ (Kornev *et al.*, 2006). This phase has also been reported in a high-pressure neutron diffraction study of PZT with $x = 0.520$ (Rouquette *et al.*, 2005).

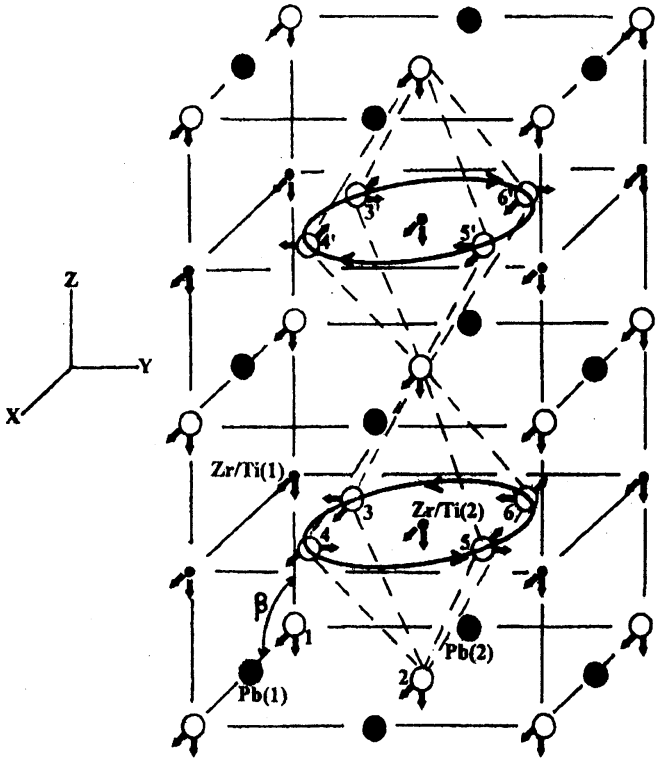


**Figure 12**
Schematic diagram of the doubled monoclinic unit cell showing superposition of anti-phase rotation of octahedra (about [001] direction) and other atoms, *i.e.* O(1), O(2), Pb(1), Pb(2), Zr/Ti(1) and Zr/Ti(2), displaced as in the *Cm* space-group model. The open circles, filled big circles and filled small circles represent O, Pb and Zr/Ti atoms, respectively. The arrows indicate the sense of displacements from their respective undisplaced position (after Ranjan *et al.,* 2002).

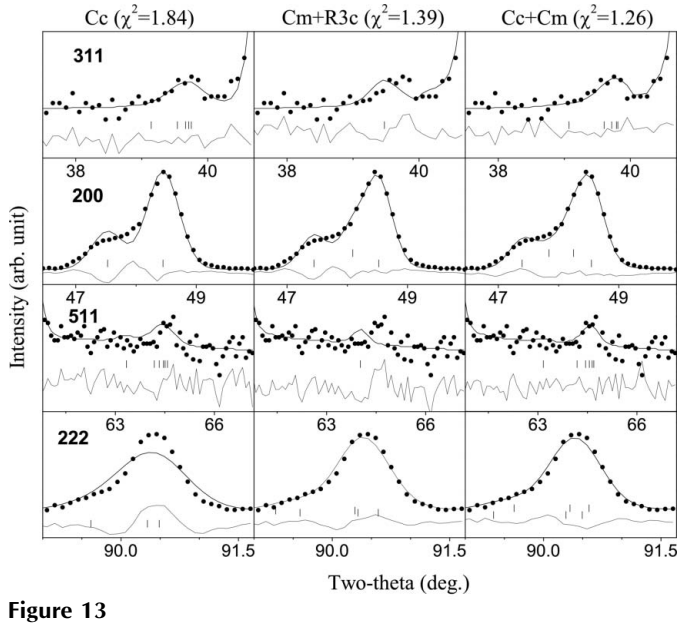


**Figure 13**
Observed (dots), calculated (solid lines) and difference (lines at the bottom) profiles for the 311 and 511 superlattice and 200 and 222 perovskite reflections of PZT with $x = 0.520$ at 10 K (after Ranjan *et al.*, 2005).

Subsequent to the above work by Ranjan *et al.* (2002) and Hatch *et al.* (2002), Frantti *et al.* (2002), while confirming the findings of Ranjan *et al.* (2002) on the appearance of the superlattice reflections in powder neutron diffraction data, proposed that the superlattice reflections are due to a rhombohedral phase in the *R*3*c* space group, which coexists with the monoclinic phase in the *Cm* space group. In view of this controversy, Ranjan *et al.* (2005) revisited the earlier Rietveld analysis using the coexistence of *R*3*c* and *Cm* phases and compared these results with those obtained for the pure *Cc* phase model (Hatch *et al.*, 2002) and also a model based on the coexistence of *Cc* and *Cm* phases (Noheda *et al.*, 2002). The results of these refinements are presented in Fig. 13 which depicts the observed, calculated and difference profiles for a few selected peaks of PZT with $x = 0.520$ at 10 K. As can be seen from this figure, the *Cc* space-group model accounts satisfactorily for the 311 and 511 superlattice reflections. The *R*3*c* model of superlattice phase along with a coexisting *Cm* phase leads to distinct mismatch between the observed and calculated peak positions for the 311 and 511 superlattice peaks. The calculated peak positions occur at lower $2\theta$ angles as compared to the observed ones. This difference in the positions of superlattice reflections is also seen in the report of Frantti *et al.* (see inset to Fig. 3 of Frantti *et al.*, 2002). It may be mentioned that Frantti *et al.* (2002) did not show the zoomed pattern of 511 superlattice reflection for which the mismatch between the observed and calculated pattern is more pronounced (see Fig. 13). Thus, the *Cm* + *R*3*c* phase model of Frantti *et al.* (2002) can be discarded. For the *Cc* phase model, although the calculated superlattice peak positions are in good agreement with those observed, the fit for the perovskite peaks like 200 and 222 is not very good. Consideration of a *Cm* phase coexisting with the *Cc* phase improves the fit for both the superlattice as well as the perovskite reflections. Thus, we can conclude that PZT with $x = 0.520$ at 10 K consists of a mixture of two phases with *Cc* and *Cm* space groups. The refined cell parameters and coordinates for the *Cc* phase obtained after the inclusion of the coexisting *Cm* phase in the Rietveld analysis are comparable to those given by Hatch *et al.* (2002). The equivalent *Cm* cell parameters obtained for the *Cc* space-group model are comparable to those of Noheda, Gonzalo *et al.* (2000). The cell parameters [$a = 5.758$ (1), $b = 5.729$ (1), $c = 4.0930$ (7) Å, $\beta = 90.59$ (1)°] of the coexisting *Cm* phase are on the other hand found to be quite different from those reported by Cox *et al.* (2005) in a similar but independent study. This coexisting *Cm* phase is similar to the room-temperature *Cm* phase reported by Ragini *et al.* (2002) for pseudorhombohedral PZT compositions with $x \geq 0.530$. As shown elsewhere (Singh *et al.*, 2007*b*), this *Cm* phase coexists with the tetragonal phase at room temperature also for $x = 0.520$ and its fraction remains constant down to 10 K, *i.e.* this coexisting phase does not take part in any of the two low-temperature phase transitions. We thus conclude that PZT with $x = 0.520$ has a monoclinic superlattice phase in the *Cc* space group, which coexists with a secondary monoclinic phase in the *Cm* space group. As shown by Ranjan *et al.* (2005), the equivalent of the refined $x$ and $z$ coordinates of all the atoms for the *Cc* space group when expressed in the *I*1*a*1 setting are very close to those obtained by Noheda, Gonzalo *et al.* (2000) for the *Cm* space group. This shows that the lower-temperature monoclinic phase in the *Cc* space group retains the main structural framework of the higher-temperature monoclinic phase with *Cm* space group. The only difference between the two phases is in the $y$ displacements of the O atoms which are responsible for the superlattice reflections (Ranjan *et al.*, 2002). Because of the low scattering factor of oxygen for X-rays, these small displacements do not lead to measurable intensities for the superlattice reflections in powder X-ray diffraction data, as a result of which Noheda *et al.* (Noheda *et al.*, 1999; Noheda, Gonzalo *et al.*, 2000; Noheda, Cox *et al.*, 2000) missed the superlattice *Cc* phase in their synchrotron XRD studies.

## 4. The outlook

It is evident from the foregoing that the structure of PZT is tetragonal ($F_T$) for $x < 0.520$ and monoclinic for $x > 0.520$ while the two phases coexist for $x = 0.520$. Thus the MPB of PZT lies around $x = 0.520$ and separates the tetragonal ($F_T$) and monoclinic ($F_M^{HT}$) phase regions, and not the tetragonal ($F_T$) and rhombohedral ($F_R^{HT}$) phase regions, believed so far in the literature (Jaffe *et al.*, 1971). The results reviewed above also reveal that the tetragonal compositions ($x \leq 0.520$) in the vicinity of the MPB undergo a succession of phase transitions from $F_T$ (*P*4*mm*) to $F_M^{HT}$ (*Cm*) to $F_M^{LT}$ (*Cc*) below room temperature. Further, the $F_M^{HT}$ phase stable at room temperature for $0.525 \leq x \leq 0.550$ transforms to $F_M^{LT}$ (*Cc*) phase on cooling below room temperature and $F_T$ (*P*4*mm*) phase on heating above room temperature. The $F_T \leftrightarrow F_M^{HT} \leftrightarrow F_M^{LT}$ transitions are accompanied by large coexistence regions indicative of their first-order character. Mishra *et al.* (1997) and Mishra & Pandey (1997) have shown that $P_C \leftrightarrow F_T$ transition for $x < 0.545$ is also first order as confirmed by discontinuous change of cell parameters and thermal hysteresis. For $x \geq 0.550$, the $F_M^{HT}$ phase (which was considered as $F_R^{HT}$ by Mishra *et al.*, 1997) transforms directly to the $P_C$ phase with no thermal hysteresis indicating second-order transition. These observations thus suggest a cross-over composition $0.545 \leq x < 0.550$ at which the paraelectric $\leftrightarrow$ ferroelectric transition may exhibit tricritical behaviour, as was first pointed out by Mishra *et al.* (1997) and Mishra & Pandey (1997). Another tricritical point towards the Zr-rich end was earlier reported by Whatmore *et al.* (1978) around $x = 0.94$.

Because of the wide coexistence region, the exact phase boundaries between various PZT phases cannot be located using diffraction data. The temperature dependence of the piezoelectric resonance frequency ($f_r$) and the elastic modulus ($1/S_{11}$) (see for example Fig. 9 for $x = 0.520$) can, however, be used to define the phase boundaries for a heating or cooling cycle rather precisely. Combining the structural and physical property measurements data, a new phase diagram of PZT around the MPB region has been constructed by Pandey & Ragini (2003) which in a slightly modified form is shown in Fig. 14. The new features of this phase diagram are the $F_T$–$F_M^{HT}$ and

$F_M^{HT}$–$F_M^{LT}$ phase boundaries below 300 K. The $F_M^{HT}$–$F_M^{LT}$ phase boundary below room temperature appears as an extrapolation of the $F_M^{LT}$–$F_M^{HT}$ phase boundary above room temperature. The $F_M^{LT}$–$F_M^{HT}$ phase boundary above room temperature has been known prior to the recent discoveries but it was labelled as the $F_R^{LT}$–$F_R^{HT}$ phase boundary (see Jaffe *et al.*, 1971). It is interesting to note from this figure that the $F_T \rightarrow F_M^{HT}(Cm) \rightarrow F_M^{LT}(Cc)$ transition on cooling below room temperature can occur up to about $x \simeq 0.48$. Further, a linear extrapolation of the $F_M^{HT}$ and $F_M^{LT}$ phase boundary up to $T = 0$ K suggests that the antiferrodistortive instability at 0 K may persist up to $x \simeq 0.31$, on the Ti-rich side of the MPB. In the composition range $0.31 \leq x \leq 0.48$, the $F_T$ phase may therefore transform under an *R*-point instability to a doubled cell structure directly without the intermediate $F_M^{HT}$ phase. Whether this phase retains the *Cc* space group confirmed experimentally for $x \geq 0.520$ or a new space group *I*4*cm*, predicted recently on the basis of first-principles calculations under virtual crystal approximation (VCA) (Kornev *et al.*, 2006), needs to be examined experimentally. Further, the experimental results, reviewed in this article do not support the existence of *R*3*m* and *R*3*c* phase regions near the MPB shown in a recently proposed phase diagram (Kornev *et al.*, 2006). The theoretical phase diagram by Kornev *et al.* (2006) contains *P*4*mm*, *Cm*, *Cc* and *I*4*cm* phase regions meeting at a point which is in obvious contradiction to the Gibbs phase rule which does not permit more than three phase regions meeting at a point in the *T*–*x* phase diagram. A careful experimental study is therefore required to settle the phase boundaries near $x = 0.48$ in Fig. 14. Woodward *et al.* (2005) have recently proposed a *Pc* space group for $0.90 \leq x \leq 0.94$ instead of *R*3*c* and *Pm* instead of *R*3*m* on the basis of indexing of the selected-area electron diffraction patterns. However, these space groups are yet to be tested using profile-fitting techniques of powder diffraction and hence we have not shown their stability fields in Fig. 14.

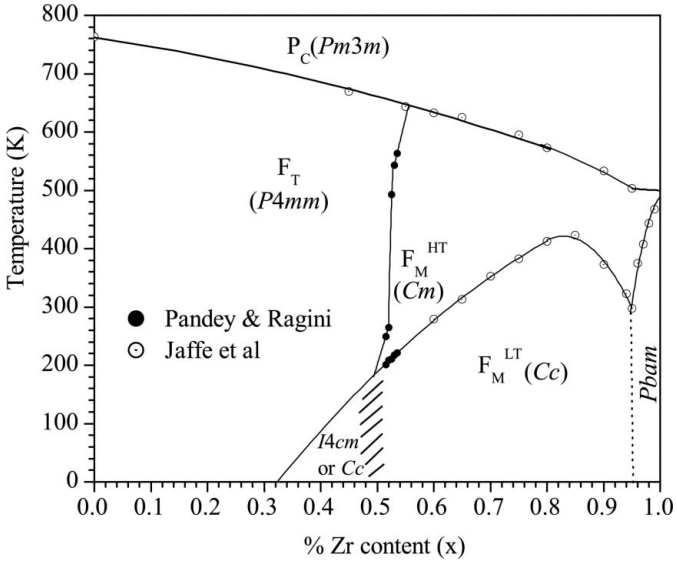


**Figure 14**
New phase diagram of PZT (after Pandey & Ragini, 2003).

The powder diffraction profiles of various pseudocubic reflections for $0.525 < x < 0.94$ resemble those for the rhombohedral structure, except for the anomalous broadening of the *h*00- (such as 200) and *hh*0- (such as 220) type reflections. The *Cm* and *Cc* monoclinic space groups for these compositions have been confirmed on the basis of the full-pattern Rietveld refinements using a rotating-anode source (Ragini *et al.*, 2002) as well as synchrotron powder XRD data (Singh *et al.*, 2007*a*,*b*). There is, however, no evidence for any splitting of the powder XRD profiles characteristic of the monoclinic *Cm* and *Cc* space groups even in the high-resolution synchrotron XRD data. This may be due to the fact that the coherently scattering domain size of the monoclinic phase in these compositions is rather small giving rise to large Scherrer broadening of various peaks, which in turn masks the monoclinic splitting of the powder XRD profiles. The fact that only certain reflections are anomalously broadened suggests that these domains are not only small but also thin-plate-like, as has recently been revealed in the TEM studies (Schönau *et al.*, 2007). On application of an intense DC electric field, some of the monoclinic domains grow at the cost of others, as a result of which the XRD peaks showing anomalous broadening in the unpoled state start exhibiting splitting characteristic of the monoclinic phase in the poled state (see *e.g.* Guo *et al.*, 2000). In the related PMN–*x*PT system, Singh *et al.* (2003) have reported characteristic monoclinic splitting of very high angle diffraction peaks in high-resolution powder neutron diffraction data for the so-called 'rhombohedral' compositions exhibiting anomalous broadening of *h*00- and *hh*0-type reflections in the powder XRD data. The high-angle peaks (pseudocubic 440, 620) resolved in the neutron data have too low an intensity in the XRD data due to the $\sin\theta/\lambda$ dependence of the atomic scattering factor ($f$). No such study has so far been carried out on PZT samples with $0.525 < x \leq 0.90$.

Wang, Khachaturyan and co-workers (Jin *et al.*, 2003; Wang, 2007) have recently advanced an adaptive phase model for the monoclinic phases of the MPB ceramics, based on the theory of martensitic transitions. In this model, the monoclinic structure observed in PZT and other MPB ceramics appears due to a conformal miniaturization of the tetragonal domains. If one accepts this picture, there should not be any tetragonal-to-monoclinic phase transition. However, Ragini *et al.* (2001) have obtained unambiguous evidence for a phase transition as revealed by anomalous softening of the elastic modulus (expressed in terms of piezoelectric resonance frequency in the original paper) as a precursor to the tetragonal-to-monoclinic *Cm* and monoclinic *Cm* to monoclinic *Cc* phase transitions followed by hardening below the phase-transition temperatures in the stability fields of the *Cm* and *Cc* phases. The Raman scattering studies also reveal appearance of new modes in confirmation of the monoclinic *Cm* and *Cc* phases (Filho *et al.*, 2000; Rouquette *et al.*, 2006). So the work of Jin *et al.* (2003) and Wang (2007) provides only a geometrical description of the monoclinic phase in terms of nanodomains of the tetragonal phase using a set of crystallographic orientation relationships; it does not preclude a phase transition for

which there is ample evidence of being driven by lattice instabilities.

The results reviewed in the preceding sections also reveal an interesting trend, pointed out by Glazer *et al.* (2004). The local structure of PZT on the tetragonal side of the MPB corresponds to short-range-ordered monoclinic regions as $Pb^{2+}$ ions are displaced from cube corners along the monoclinic ⟨100⟩ directions (Noheda, Gonzalo *et al.*, 2000; Ragini *et al.*, 2002). The structure becomes truly long ranged monoclinic in the MPB region as shown in §2.2.1 for $x = 0.525$. Finally, it becomes short-ranged monoclinic for the Zr-rich compositions ($x > 0.525$) as indicated by the anomalous broadening of the *h*00- and *hh*0-type peaks. The absence of the rhombohedral phase on the Zr-rich side of the MPB for $x > 0.525$ suggests that the original idea of the monoclinic phase stable only in a narrow composition range near MPB as a bridging phase [see *e.g.* the recent reviews by Noheda (2002) and Noheda & Cox (2006)] between the tetragonal and rhombohedral phases is untenable. Further, in the absence of the rhombohedral phases on the Zr-rich side, the polarization rotation model of high piezoelectricity (Fu & Cohen, 2000; Bellaiche *et al.*, 2000) loses relevance for PZT. A similar situation seems to exist in PMN–*x*PT also (Singh & Pandey, 2005; Singh *et al.*, 2006), where the so-called 'rhombohedral' phase turns out to be monoclinic (see Singh *et al.*, 2006 for the latest phase diagram).

The results presented in this overview are based on collaborations with S. K. Mishra, A. P. Singh, R. Lal, Ch. Durga Prasad, Ragini, R. Ranjan, H. Lemmens, G. Van Tendeloo, B. J. Kennedy, D. M. Hatch, H. T. Stokes, S. Yoon and N. Shin. DP gratefully acknowledges their valuable contributions in settling the subtle aspects of PZT. This article has been prepared on the basis of the recommendations of the IUCr Commission on Inorganic and Mineral Structures for which DP is grateful to the Chairman (Professor G. Ferraris) and the members of this Commission.

## References

Ari-Gur, P. & Benguigui, L. (1974). *Solid State Commun.* **15**, 1077–1079.
Bellaiche, L., Garcia, A. & Vanderbilt, D. (2000). *Phys. Rev. Lett.* **84**, 5427–5430.
Bonny, V., Bonin, M., Sciau, Ph., Schenk, K. J. & Chapuis, G. (1997). *Solid State Commun.* **102**, 347–352.
Bruce, A. D. & Cowley, R. A. (1980). *Adv. Phys.* **29**, 219–321.
Clarke, R. & Glazer, A. M. (1976). *Ferroelectrics*, **12**, 207–209.
Corker, D. L., Glazer, A. M., Whatmore, R. W., Stallard, A. & Fauth, F. (1998). *J. Phys. Condens. Matter*, **10**, 6251–6269.
Cox, D. E., Noheda, B. & Shirane, G. (2005). *Phys. Rev. B*, **71**, 134110.
Filho, A. G. S., Lima, K. C. V., Ayalya, A. P., Guedes, I., Freire, P. T. C., Filho, J. M., Araujo, E. B. & Eiras, J. A. (2000). *Phys. Rev. B*, **61**, 14283–14286.
Fornari, M. & Singh, D. J. (2001). *Phys. Rev. B*, **63**, 092101.
Frantti, J., Ivanov, S., Eriksson, S., Rundolf, H., Lantto, V., Lappalainen, J. & Kakihana, M. (2002). *Phys. Rev. B*, **66**, 064108.
Fu, H. & Cohen, R. E. (2000). *Nature (London)*, **403**, 281–283.
Glazer, A. M. (1972). *Acta Cryst.* B**28**, 3384–3392.
Glazer, A. M., Mabud, S. A. & Clarke, R. (1978). *Acta Cryst.* B**34**, 1060–1065.
Glazer, A. M., Thomas, P. A., Baba-Kishi, K. Z., Pang, G. K. H. & Tai, C. W. (2004). *Phys. Rev. B*, **70**, 184123.
Guo, R., Cross, L. E., Park, S.-E., Noheda, B., Cox, D. E. & Shirane, G. (2000). *Phys. Rev. Lett.* **84**, 5423–5426.
Hatch, D. M., Stokes, H. T., Ranjan, R., Ragini, Mishra, S. K., Pandey, D. & Kennedy, B. J. (2002). *Phys. Rev. B*, **65**, 212101.
Howard, C. J., Kennedy, B. J. & Chakoumakos, B. C. (2000). *J. Phys. Condens. Matter*, **12**, 349–365.
*International Tables for Crystallography* (2005). Vol. A. Dordrecht: Kluwer Academic Publishers.
Isupov, V. A. (1968). *Sov. Phys. Solid State*, **10**, 989.
Jaffe, B., Cook, W. R. & Jaffe, H. (1971). *Piezoelectric Ceramics*. London, New York: Academic Press.
Jin, Y. M., Wang, Y. U., Khachaturyan, A. G., Li, J. F. & Viehland, D. (2003). *Phys. Rev. Lett.* **91**, 197601.
Jona, F. & Shirane, G. (1962). *Ferroelectric Crystals*. Oxford: Pergamon Press.
Kennedy, B. J., Howard, C. J. & Chakoumakos, B. C. (1999). *J. Phys. Condens. Matter*, **11** 1479–1488.
Kiat, J. M., Uesu, Y., Dkhil, B., Matsuda, M., Malibert, C. & Calvarin, G. (2002). *Phys. Rev. B*, **65**, 064106.
Kornev, I. A., Bellaiche, L., Janolin, P.-E., Dkhil, B. & Suard, E. (2006). *Phys. Rev. Lett.* **97**, 157601.
Lampis, N., Sciau, Ph. & Lehmann, A. G. (1999). *J. Phys. Condens. Matter*, **11**, 3489–3500.
Lines, M. E. & Glass, A. M. (1977). *Principles and Applications of Ferroelectrics and Related Materials*. Oxford: Clarendon.
Mishra, S. K. & Pandey, D. (1997). *Philos. Mag. B*, **76**, 227–240.
Mishra, S. K., Pandey, D. & Singh, A. P. (1996). *Appl. Phys. Lett.* **69**, 1707–1709.
Mishra, S. K., Singh, A. P. & Pandey, D. (1997). *Philos. Mag. B*, **76** 213–226.
Noheda, B. (2002). *Curr. Opin. Solid State Mater. Sci.* **6**, 27–34.
Noheda, B. & Cox, D. E. (2006). *Phase Transit.* **79**, 5–20.
Noheda, B., Cox, D. E., Shirane, G., Gonzalo, J. A., Cross, L. E. & Park, S.-E. (1999). *Appl. Phys. Lett.* **74**, 2059–2061.
Noheda, B., Cox, D. E., Shirane, G., Guo, R., Jones, B. & Cross, L. E. (2000). *Phys. Rev. B*, **63**, 014103.
Noheda, B., Gonzalo, J. A., Cross, L. E., Guo, R., Park, S.-E., Cox, D. E. & Shirane, G. (2000). *Phys. Rev. B*, **61**, 8687–8695.
Noheda, B., Wu, L. & Zhu, Y. (2002). *Phys. Rev. B*, **66**, 060103.
Pandey, D. & Ragini (2003). *Z. Kristallogr.* **218**, 1–7.
Ragini, Mishra, S. K., Pandey, D., Lemmens, H. & Van Tendeloo, G. (2001). *Phys. Rev. B*, **64**, 054101.
Ragini, Ranjan, R., Mishra, S. K. & Pandey, D. (2002). *J. Appl. Phys.* **92**, 3266–3274.
Ranjan, R., Ragini, Mishra, S. K., Pandey, D. & Kennedy B. J. (2002). *Phys. Rev. B*, **65**, 060102.
Ranjan, R., Singh, A. K., Ragini & Pandey, D. (2005). *Phys. Rev. B*, **71**, 092101.
Rouquette, J., Haines, J., Bornand, V., Pintard, M., Papet, Ph., Marshall, W. G. & Hull, S. (2005). *Phys. Rev. B*, **71**, 024112.
Rouquette, J., Haines, J., Bornand, V., Pintard, M., Papet, Ph. & Sauvajol, J. L. (2006). *Phys. Rev. B*, **73**, 224118.
Schönau, K. A., Schmitt, L. A., Knapp, M., Fuess, H., Eichel, R.-A., Kungl, H. & Hoffmann, M. J. (2007). *Phys. Rev. B*, **75**, 184117.
Singh, A. P., Mishra, S. K., Pandey, D., Prasad, Ch. D. & Lal, R. (1993). *J. Mater. Sci.* **28**, 5050–5055.
Singh, A. K. & Pandey, D. (2001). *J. Phys. Condens. Matter*, **13**, L931–L936.
Singh, A. K. & Pandey, D. (2003). *Phys. Rev. B*, **67**, 064102.
Singh, A. K. & Pandey, D. (2005). *Ferroelectrics*, **326**, 91–99.
Singh, A. K., Pandey, D., Yoon, S., Shin, N. & Baik, S. G. (2007*a*) *Appl. Phys. Lett.* **91**, 192904.
Singh, A. K., Pandey, D., Yoon, S., Shin, N. & Baik, S. G. (2007*b*). In preparation.

Singh, A. K., Pandey, D. & Zaharko, O. (2003). *Phys. Rev. B*, **68**, 172103.
Singh, A. K., Pandey, D. & Zaharko, O. (2006). *Phys. Rev. B*, **74**, 024101.
Stephens, P. W. (1999). *J. Appl. Cryst.* **32**, 281–289.
Stokes, H. T. & Hatch, D. M. (2000). *ISOTROPY*. Software and documentation is available at http://www.physics.byu.edu/~stokesh/isotropy.html.
Thapa, K. B. (1998). MSc Physics Dissertation, Banaras Hindu University, India.
Vanderbilt, D. & Cohen, M. H. (2001). *Phys. Rev. B*, **63**, 094108.
Wang, Y. U. (2007). *Phys. Rev. B*, **76**, 024108.
Whatmore, R. W., Clarke, R. & Glazer, A. M. (1978). *J. Phys. C Solid State Phys.* **11**, 3089–3102.
Woodward, D. I., Knudsen, J. & Reaney, I. M. (2005). *Phys. Rev. B*, **72**, 104110.